

OPTICAL AND INFRARED OBSERVATIONS OF THE SUPERNOVA SN 1999el¹

E. DI CARLO,² F. MASSI,² G. VALENTINI,² A. DI PAOLA,³ F. D’ALESSIO,³ E. BROCATO,² D. GUIDUBALDI,² M. DOLCI,²
F. PEDICHINI,³ R. SPEZIALI,³ G. LI CAUSI,³ A. CARATTI O GARATTI,² E. CAPPELLARO,⁴ M. TURATTO,⁴ A. A. ARKHAROV,⁵
Y. GNEDIN,⁵ V. M. LARIONOV,^{5,6,7} S. BENETTI,^{4,8} A. PASTORELLO,⁴ I. ARETXAGA,^{9,10} V. CHAVUSHYAN,^{9,10} O. VEGA,^{9,10}
I. J. DANZIGER,¹¹ AND A. TORNAMBÉ²

Received 2001 September 12; accepted 2002 March 5

ABSTRACT

Optical and near-infrared light curves of the Type II_n supernova SN 1999el in NGC 6951 are presented. A period of 220 days (416 days in the near-infrared) is covered from the first observation obtained a few days before maximum light. Spectroscopic observations are also discussed. Using as a distance calibrator the Type Ia SN 2000E, which occurred some months later in the same galaxy, and fitting a blackbody law to the photometric data, we obtain a maximum bolometric luminosity for SN 1999el of $\sim 10^{44}$ ergs s⁻¹. In general, the photometric properties of SN 1999el are very similar to those of SN 1998S, a bright and well-studied Type II_n supernova, showing a fast decline in all observed bands similar to those of Type II-L supernovae. The differences with SN 1998S are analyzed and ascribed to the differences in a preexisting circumstellar envelope in which dust was already present at the moment of the SN outburst. We infer that light echoes may play a possibly significant role in affecting the observed properties of the light curves, although improved theoretical models are needed to account for the data. We conclude that mass loss in the progenitor RG stars is episodic and occurs in an asymmetric way. This implies that collapsing massive stars appear as normal Type II supernovae if this occurs far from major mass-loss episodes, whereas they appear as Type II_n supernovae if a large mass-loss episode is in progress.

Subject headings: galaxies: individual (NGC 6951) — infrared: stars — supernovae: general — supernovae: individual (SN 1999el)

1. INTRODUCTION

A significant fraction of the total number of Type II supernovae (SNe II) show distinctive features that led Schlegel (1990) to introduce the class of SNe II_n. These objects are characterized by a blue continuum near maximum and a slow temporal evolution of the spectrum; the slowly declining luminosity in the optical bands and the narrow H α line profile superposed on a broad base indicate the presence of diffuse lower velocity matter around the site of the explosion. Because of their relatively high luminosity and slowly declining light curve, the SNe II_n are easier to discover than

faint, narrow-peak light-curve objects. Their intrinsic frequency has been estimated by Cappellaro et al. (1997) to be 5% of all SNe II. There is, however, a marked inhomogeneity among the events (Cappellaro & Turatto 2001), namely, concerning the decline rate of the light curves, a matter that merits understanding. It has not yet been clarified to what extent individual differences among members of this type of supernova can be totally ascribed to the physical properties of preexisting circumstellar matter (CSM).

In fact, recent attempts to explain the long-term properties of visual light curves (LCs) with light echoes from circumstellar matter by Roscherr & Schaefer (2000) have not been fully successful. There are observational features that disagree with echo model predictions, forcing these authors to conclude that any preexisting dust around the site of the explosion must be almost completely destroyed at the moment of the outburst. However, this contrasts with the observed late-infrared emission from SN 1998S, which has been inferred to result from dust cooling (Fassia et al. 2000). On the basis of their observational data, Fassia et al. argue that dust was already present within the precursor wind of SN 1998S, and hence at least a fraction of it must have survived the explosion. This suggests that improved observations are needed in order to understand the environment of SN sites from this diagnostic tool. So far only a few of the models developed to test the effects of light echoes have taken into account the near-infrared (NIR) light curves (see Emmering & Chevalier 1988).

On the other hand, the slow decline of light curves for SNe II_n appears to be well accounted for by simple models of ejecta-wind interactions (Terlevich 1994; Chugai 1990, 1992). At the same time, the peculiar shape of the emission lines has also been attributed to ejecta-wind interactions involving a two-component wind, characterized by dense

¹ Based on observations collected with the AZT-24 telescope (Campo Imperatore, Italy), the 1.8 m telescope of the Osservatorio Astronomico di Padova (Asiago, Italy), the Teramo-Normale Telescope operated by the Osservatorio Astronomico di Collurania-Teramo (Teramo, Italy), the Italian Telescopio Nazionale Galileo (La Palma, Canary Islands, Spain), the 1 m telescope of the Observatorio Astronómico Nacional (Tonantzintla, Mexico), and the 2.1 m telescope of the Guillermo Haro Observatory (Cananea, Mexico).

² Osservatorio Astronomico di Collurania-Teramo, Via M. Maggini, I-64100 Teramo, Italy; dicarlo@te.astro.it.

³ Osservatorio Astronomico di Roma, Via Frascati 33, I-00040 Monteporzio Catone (Rome), Italy.

⁴ Osservatorio Astronomico di Padova, Vicolo dell’ Osservatorio 5, I-35122 Padua, Italy.

⁵ Central Astronomical Observatory at Pulkovo, Pulkovskoe shosse 65, 196140 Saint Petersburg, Russia.

⁶ Astronomical Institute of St. Petersburg University, Russia.

⁷ Isaac Newton Institute of Chile, St. Petersburg branch.

⁸ Telescopio Nazionale “Galileo,” Apartado de Correos 565, E-38700 Santa Cruz de La Palma, Canary Islands, Spain.

⁹ Instituto Nacional de Astrofísica, Óptica y Electrónica, Apartado Postal 51 y 216, Puebla, Mexico.

¹⁰ Instituto Nacional de Astrofísica, Óptica y Electrónica INAOE, S.M. de Tonantzintla, Puebla, Mexico.

¹¹ Osservatorio Astronomico di Trieste, Via G.B. Tiepolo 11, I-34131 Trieste, Italy.

clumps (or a dense equatorial wind) associated with a less dense spherically symmetric distribution (Chugai & Danziger 1994).

Therefore, several open questions remain, which can be formulated as follows:

1. How important is the issue of the inhomogeneity of this class of events, and what causes this inhomogeneity?
2. What is the evolutionary scenario causing some massive precursors of SNe to explode within a preexisting envelope of diffuse CSM, and what physical mechanisms affect the observational properties?
3. Is dust present in the CSM before the explosion?
4. To what extent do echo processes and ejecta-wind interactions determine the observational properties of such SNe?

In this paper we present optical and infrared data for the Type II_n SN 1999el. The present work provides new photometric measurements and improves the observational constraints on this class of SNe. Observations and data reduction are presented in § 2. The results are presented and discussed in §§ 3 and 4 and summarized in § 5.

2. OBSERVATIONS AND DATA REDUCTION

SN 1999el was discovered on October 20.45 UT (JD 2,451,472) at ~ 15.4 mag (unfiltered) by the Beijing Astronomical Observatory (BAO) Supernova Survey (Cao et al. 1999; IAUC 7288) $\sim 23''$ east and $\sim 9''$ south of the galactic

nucleus of NGC 6951, an inclined ($i = 42^\circ$) barred spiral galaxy hosting a type 2 Seyfert AGN located at $\alpha(1950) = 20^{\text{h}}36^{\text{m}}36^{\text{s}}.59$ and $\delta(1950) = +65^\circ55'46''00$ (see Fig. 1). (For a list of galactic properties see, e.g., Kohno, Kawabe, & Vila-Vilaró 1999 and references therein.) The distance to NGC 6951 was recently discussed by Vinkó et al. (2001). The estimated distance moduli range from 31.85 mag (23.4 Mpc) to 32.59 mag (33 Mpc), where the lowest values are based on the Tully-Fisher relation and the highest ones on the multicolor light-curve shape method applied to the SN 2000E (an SN Ia). We adopt our own determination (32.1 ± 0.4 mag) based on our observations of SN 2000E (see G. Valentini et al. 2002, in preparation).

Cao et al. (1999) report no trace of the SN on images taken on October 19.2 by the Katzman Automatic Imaging Telescope (to a limiting magnitude of 18) and on October 19.44 by BAO, so we can assume October 20.00 as the zero point for the light curves, since it must be very close (within a few hours) to the shock breakout time. According to Cao et al. (1999), an image taken on October 21.44 indicates a magnitude of 15.0 for the supernova, whereas on October 22.2 it appeared at a magnitude of 15.2 (no band is indicated). It can be seen from Figure 1 that SN 1999el is projected between two nearby foreground stars (c2 and c3) with a separation of no more than a couple of arcseconds.

2.1. Optical Data: Acquisition, Reduction, and Photometry

Optical photometry of SN 1999el has been obtained on images collected with several telescopes at different sites in

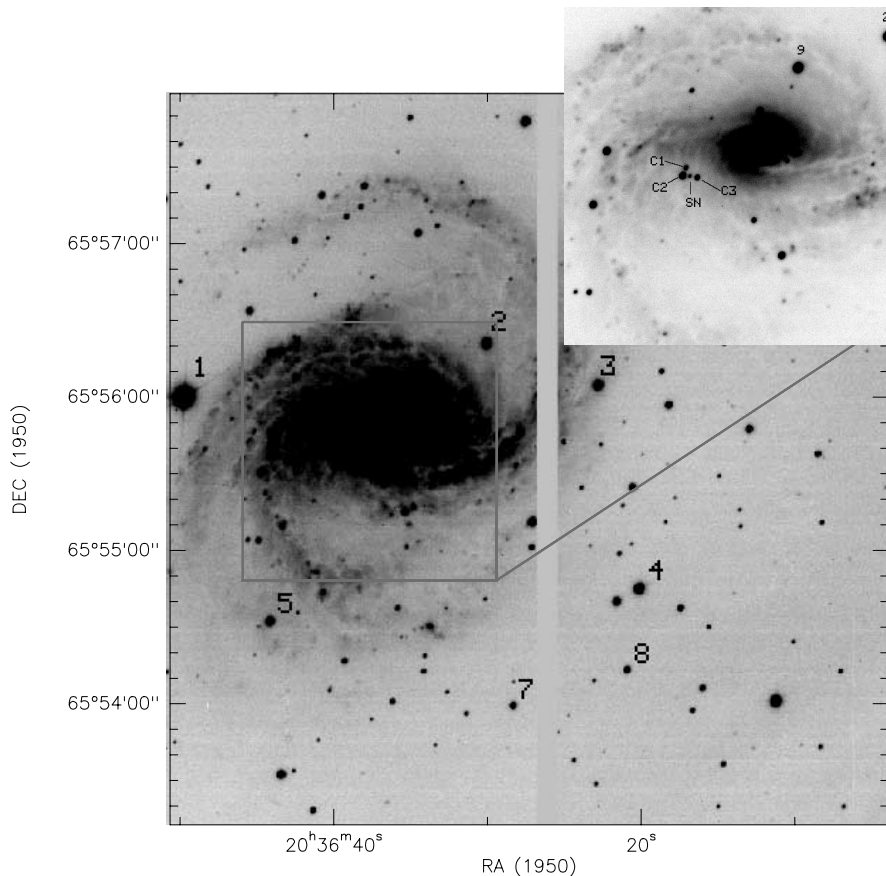


FIG. 1.—*V*-band image of SN 1999el in the galaxy NGC 6951 obtained at the TNG on JD 2,451,690. Stars of the local sequence are indicated by numbers (star 6 is out of the displayed field). The enlarged box shows the supernova, which lies toward a group of close projected stars referred to as c1, c2, and c3 in the text.

the northern hemisphere. These were reduced using the standard techniques for debiasing and flat-fielding.

One set of data comes from the 0.72 m Teramo-Normale Telescope (TNT) at the Teramo Observatory (Italy). TNT is an $f/14$ Ritchey-Chretien reflector equipped with a Tektronic Tk512 CB1-1 front-illuminated 512×512 pixel CCD. The pixel size of $27 \mu\text{m}$ yields a scale of $0''.46 \text{ pixel}^{-1}$. During each observational night we obtained 4–12 frames per filter in the B , R , and I bands.

Other photometry was performed on images obtained with the 1 m telescope operated by the Observatorio Astronómico Nacional in Tonantzintla (Mexico), equipped in the $f/15$ Cassegrain port with a 1024×1024 Thomson THX 31156 CCD and a Cousins R filter. The field of view covered by this configuration is $4'.2 \times 4'.2$. The chip was binned 2×2 and read in standard mode ($3.47 e^- \text{ pixel}^{-1}$, $2.7 e^- \text{ ADU}^{-1}$). The effective on-chip integration of the SN field was split into 3–6 on-chip integrations of 300 s, offset from each other by $\sim 20''$.

For imaging, the 1.8 m telescope of the Osservatorio Astronomico di Padova sited in Asiago, Cima Ekar (Italy), equipped with AFOSC, was also used. The instrument is a focal reducer–type spectrograph/camera with a $1 \text{ K} \times 1 \text{ K}$ site-thinned CCD ($24 \mu\text{m}$). The scale of $0''.473 \text{ pixel}^{-1}$ gives a field of $8 \times 8 \text{ arcmin}^2$.

Some photometric data were acquired using the 2.1 m telescope of the Guillermo Haro Observatory in Cananea (Mexico), equipped with the spectrophotometer LFOSC at the $f/12$ Cassegrain focus. Johnson V and Cousins R filters were used. The chip is a 385×578 EEV P8693, with a field of view of $6' \times 10'$. This was read in the standard readout mode: $8 e^- \text{ pixel}^{-1}$, $4.7 e^- \text{ ADU}^{-1}$. The effective on-chip integration of the SN field was split into 2–3 integrations of 60 s in the R band and of 120 s in the V band.

Late-time $UBVRI$ photometry was obtained with the Optical Imager Galileo mounted on the 3.58 m Italian Telescopio Nazionale Galileo (TNG), La Palma, Canary Islands, and equipped with a mosaic of two thinned, back-illuminated EEV42-80 CCDs with 2048×4096 pixels each (pixel size $13.5 \mu\text{m}$; pixel scale in 2×2 binned mode $0''.144 \text{ pixel}^{-1}$). These nights were photometric and were used to calibrate the local sequence around the SN (1–8, see Fig. 1), which in turn was used for calibrating nonphotometric nights. The instrumental color equations were obtained through observations of stars in the standard fields of Landolt (1992). Three of the local standards (stars 1, 3, and 5) are a subset of those selected by Vinkó et al. (2001) to carry out differential photometry ($BVRI$) on SN 2000E (their stars F1, B1, and B3, respectively). The magnitudes adopted in our and their study for those sources agree within 0.05 mag, with two exceptions: we found our star 1 to be 0.13 mag brighter in R and our star 5 to be 0.13 mag brighter in I . The agreement can be considered good and confirms the validity of both our calibration and that of those authors. However, our measurements were obtained using a larger telescope (the TNG) under very good seeing and photometric conditions. This should have afforded us a better sky subtraction that, particularly at longer wavelengths, may be easily affected by nebular emission from the host galaxy.

During the SN 1999el follow-up observations, another SN event occurred within NGC 6951 (i.e., SN 2000E), so the CCD at TNT was operated to image the two objects on the same frame. The exposure times were chosen so as to achieve the best signal-to-noise ratio (S/N) for both super-

novae but avoiding saturation of the brightest calibration star in the field.

Since both supernovae are well embedded in the galaxy background, we obtained instrumental magnitudes by point-spread function (PSF) fitting using the DAOPHOT package in IRAF or a set of procedures developed for SN photometry in the same environment. For the TNT and Tonantzintla observations, the final instrumental magnitudes were obtained as an average of all valid values derived for a given night.

Errors have been obtained with artificial star experiments, i.e., placing stars of the same magnitude as the supernova in parts of the galaxy arm characterized by similar complexity as the SN site, then computing the rms of the derived magnitudes. For TNT images, however, the uncertainty in the photometry has been estimated by evaluating the PSF fit residuals and the rms of the n successive measurements obtained in a single night for the SN after calibration through the local standards. It is more difficult to assess the error because of the convolution of the PSFs of the SN and the nearby sources when their brightness becomes comparable and the seeing is poor, which is the case in the TNT photometry at late epochs. Hence, we omit measurements that appear uncertain because of the inferior quality of the images. Table 1 lists the results of optical photometry for SN 1999el.

2.2. Infrared Data: Acquisition, Reduction, and Photometry

Most NIR observations of SN 1999el were obtained at the AZT-24 1.1 m telescope in Campo Imperatore (Italy) with SWIRCAM, during a period spanning 1999 October 25 to 2000 May 26. SWIRCAM (D'Alessio et al. 2000) incorporates a 256×256 HgCdTe NICMOS 3-class (PICNIC) detector that, at the focus of AZT-24, yields a scale of $1''.04 \text{ pixel}^{-1}$, resulting in a field of view of $\sim 4 \times 4 \text{ arcmin}^2$. The observations were performed through standard J ($1.25 \mu\text{m}$), H ($1.65 \mu\text{m}$), and K ($2.20 \mu\text{m}$) broadband filters. Any on-source image was obtained as a median composition of five frames with a $15''$ dithering and integration times of 60 s each at the J and H bands, and 120 s each at the K band. Off-source frames were taken with a $10'$ offset with the same observational procedure and exposure times but a larger ($50''$) dithering. Sky images obtained as a median of the original dithered off-source frames were subtracted from the single on-source images before composition.

Flat-field frames were acquired at twilight using the differential flat technique that relies on the natural variation of the sky background. In this way, the frames with the highest mean counts are combined together (through median filtering) in one single image, as are those with the lowest mean counts, and the resultant lower signal image is subtracted from the resultant higher signal one so as to remove any biases and dark current. This is used to flat-field each image after sky subtraction.

Deep JHK_s images of SN 1999el were obtained at the 3.58 m TNG telescope (La Palma) with ARNICA during the night of 2000 May 26. ARNICA is a 256×256 pixel NIR camera (Lisi et al. 1996) and was matched to the TNG with a $0''.35 \text{ pixel}^{-1}$ scale (yielding a $90'' \times 90''$ field of view). Sequences of four dithered on-source and four off-source images were taken moving the telescope to a sky position after each on-source integration. Total on-source integration times amounted to 12 minutes at K_s and 8 minutes at

TABLE 1
UBVR PHOTOMETRY FOR SN 1999el OBTAINED WITH DIFFERENT INSTRUMENTS

JD (2,451,000+)	Epoch (days)	<i>U</i> (mag)	ΔU (mag)	<i>B</i> (mag)	ΔB (mag)	<i>V</i> (mag)	ΔV (mag)	<i>R</i> (mag)	ΔR (mag)	<i>I</i> (mag)	ΔI (mag)	Telescope
479.42	7.42	15.87	0.06	14.71	0.04	14.35	0.03	TNT
480.45	8.45	15.87	0.03	14.68	0.04	14.31	0.02	TNT
481.58	9.58	14.69	0.02	Tonantzintla
485.31	13.31	15.83	0.03	14.60	0.03	14.22	0.03	TNT
486.25	14.25	15.82	0.06	14.56	0.06	14.25	0.02	TNT
486.50	14.50	15.70	0.05	15.73	0.05	15.11	0.04	14.65	0.03	14.19	0.05	TNG
486.52	14.52	14.59	0.02	Tonantzintla
486.57	14.57	15.04	0.03	14.59	0.20	Cananea
490.48	18.48	15.65	0.03	15.64	0.06	14.98	0.02	14.52	0.04	13.99	0.03	Asiago
490.57	18.57	14.92	0.02	14.48	0.04	Cananea
493.60	21.57	14.55	0.04	Tonantzintla
498.68	26.68	14.55	0.02	Tonantzintla
506.21	34.21	16.41	0.06	14.86	0.06	14.46	0.03	TNT
513.59	41.59	15.08	0.10	Tonantzintla
514.25	42.25	16.76	0.06	15.20	0.04	TNT
516.53	44.53	15.13	0.02	Tonantzintla
520.21	48.21	17.14	0.04	15.51	0.08	14.85	0.02	TNT
521.23	49.23	17.17	0.06	15.58	0.06	15.01	0.03	TNT
522.54	50.54	15.33	0.03	Tonantzintla
531.29	59.29	17.52	0.08	16.03	0.10	TNT
561.25	89.25	19.44	0.30	17.54	0.20	TNT
570.27	98.27	19.67	0.20	18.40	0.20	17.54	0.07	TNT
571.25	99.25	18.94	0.26	18.46	0.14	Asiago
572.24	100.24	19.83	0.20	18.69	0.20	17.64	0.08	TNT
575.29	103.24	20.19	0.20	19.19	0.25	18.25	0.18	17.53	0.22	Asiago
585.30	113.30	20.27	0.16	19.22	0.16	18.42	0.24	17.78	0.16	Asiago
604.50	132.50	21.27	0.40	20.97	0.30	19.52	0.25	18.89	0.15	18.03	0.10	TNG
605.50	133.50	> 19.17	...	19.27	0.30	TNG
690.50	218.50	21.44	0.20	21.54	0.15	20.49	0.10	19.83	0.10	18.91	0.15	TNG
698.54	226.54	21.44	0.40	20.45	0.30	19.81	0.30	18.90	0.25	Asiago
699.55	227.55	21.42	0.30	20.56	0.30	19.77	0.30	Asiago

J and *H*. Five images per band of a group of standard stars (AS 40-5, AS 40-0, and AS 40-1; Hunt et al. 1998) were also obtained so as to locate the brightest of them (AS 40-5) at the center of the array and of each detector quadrant in turn. Flat-field frames in the K_s band were taken at sunset. Only the K_s frames were sky-subtracted after flat-fielding; off-source images (or the dithered ones for standard stars) were combined together and used for flat-fielding in the *J* and *H* bands. All images in each band were finally corrected for bad pixels, registered, and averaged together.

Late-time NIR images were acquired with the Near Infrared Camera and Spectrograph (NICS) at the TNG on 2000 December 14 (JD + 893) during the commissioning of the camera. NICS is based on a 1024×1024 Hawaii detector (Baffa et al. 2001), and we employed a $0''.25$ pixel $^{-1}$ scale resulting in a field of view of 4.2×4.2 arcmin 2 . Dithered on-source and off-source frames were taken in the J_s and K' bands with total (on-source) integration times of 1200 and 420 s, respectively. Data were reduced as described above, but no flat-field frames were available for K' images.

The photometric measurements on SWIRCAM images were performed by PSF fitting using the DAOPHOT package in MIDAS in order to derive relative photometry between the supernova and a set of comparison stars properly selected in the field among the ones with the highest S/N (stars 1–9 in Fig. 1), of which those calibrated with the TNG data (see below) are a subset. For these, variability could be ruled out on the basis of an accurate image-by-

image check of the fluctuations in their relative magnitudes. PSF-fitting photometry was also needed owing to the partial convolution of the SN with the sources c1, c2, and c3 of Figure 1.

The presence of the parent galaxy background has been taken into account by evaluating its influence on the derived photometry of the SN. In particular cases, i.e., when the S/N was low, PSF-fitting photometry was carried out using the ROMAFOT package in MIDAS by means of which the background gradient due to the diffuse emission from the galaxy was accounted for by adopting a tilted plane.

Both aperture and PSF-fitting photometry were performed on the ARNICA images for field stars using the package DAOPHOT in IRAF (Stetson 1987). However, we obtained more satisfactory PSF fits to SN 1999el using the package ROMAFOT in MIDAS. The group of three stars, close in projection to the supernova and all resolved on the TNG images (see Fig. 1), is composed of, following the nomenclature used in the figure, c2 ($K_s = 14.97 \pm 0.03$), $\sim 2''$ east of the SN, c3 ($K_s = 16.75 \pm 0.32$), $\sim 2''$ west of the SN, and c1 ($K_s \sim 19$). The observed standard stars were used to calibrate both the SN and the field stars 2 and 9 (see Fig. 1), which served as references for the photometry on SWIRCAM frames. K_s magnitudes were converted into K magnitudes by extrapolating the continuum flux within the spectral region ($\sim 0.1 \mu\text{m}$ wide) of K not covered by the K_s filter, with corrections amounting to ≤ 0.02 mag for the standard stars and to 0.06 mag for SN 1999el (the uncor-

rected sources being fainter). Possible CO molecular line emission falling out of K_s but within K , and sometimes occurring in the case of SNe IIn, was therefore not detected and could not account for any fraction of the measured flux. The photometry of the standard stars for the five positions on the array indicates that residual errors of ~ 0.05 , ~ 0.04 , and ~ 0.02 mag in the J , H , and K_s bands, respectively, are still present because of flat-field inaccuracies.

Differential photometry on the NICS images was performed by PSF fitting using ROMAFOT in MIDAS. By intercomparing instrumental magnitudes obtained both for the field (and local standard) stars and for the close-by sources (c1–c3), we checked that even though not flat-fielded, K' -values were consistent at a 0.1–0.2 mag level with ARNICA photometry throughout the whole final frame. We conservatively assumed uncertainties ~ 0.5 mag both for J_s and for K' and did not correct for the slight differences with the J and K bands. Table 2 lists the results of NIR photometry for SN 1999el.

2.3. Spectroscopy

Two spectra of the SN have been obtained a few hours apart in Asiago (1999 November 7) and Cananea (November 8), i.e., about 18 days after the discovery. In Figure 2 we show the latter obtained with a $5.5 \text{ \AA pixel}^{-1}$ grism, which for a $3''$ slit-width, yields a resolution of $\sim 16 \text{ \AA}$ in the 4000–7200 \AA range. The total 4400 s exposure was split into three integrations to minimize the effect of cosmic rays. Wavelength calibrations were obtained using comparison spectra of HeArNe lamps, while the instrumental signature has been removed using a spectrophotometric standard star.

3. RESULTS AND ANALYSIS

3.1. Optical Spectrum

The spectrum (Fig. 2) confirms the early finding by Filippenko, as quoted in Cao et al. (1999), that the SN shows lines with narrow components. Superposed on the continuum there are strong, relatively narrow Balmer emission lines of H together with wider weak wings. The broad wings could be fitted with Gaussian profiles having FWHM of about 2500–3000 km s^{-1} , while the narrow ones are barely resolved. Also, narrow P Cygni absorption components with minima displaced by about 600–900 km s^{-1} relative to the emission-line cores are present, indicating a slowly expanding shell of gas above the photosphere. Fe II lines have similar structures. Weak Na I D lines are visible.

In Figure 2 we compare the spectrum of SN 1999el with those of other H-dominated SNe at similar epochs showing signs of interaction with the CSM. The SN 1999el spectrum is very different from the spectra of SN 1988Z, the best-studied SN IIn (Stathakis & Sadler 1991; Turatto et al. 1993; Chugai & Danziger 1994; Aretxaga et al. 1999). The line widths of SN 1988Z are much broader, implying expansion velocities of about 15,000 km s^{-1} . On the contrary, the spectrum of SN 1999el closely resembles those of SN 1999eb and SN 1995G (A. Pastorello et al. 2002, in preparation) at comparable age. They have similar continua, strong emission lines with similar profiles, and narrow absorption components. It is the very narrow blueshifted absorption component, particularly in the wing of the broad $H\alpha$ from the expanding envelope, that is characteristic of a class of SNe, such as SN 1996L (Benetti et al. 1999), SN 1994aj (Benetti et al. 1998), and SN 1984E (Dopita et al. 1984).

TABLE 2
NIR PHOTOMETRY OF SN 1999el OBTAINED WITH SWIRCAM, ARNICA, AND NICS

Julian Day (2,451,000+)	Epoch (days)	J (mag)	ΔJ (mag)	H (mag)	ΔH (mag)	K (mag)	ΔK (mag)	Telescope
477.31	5.31	13.69	0.03	13.30	0.05	12.70	0.09	AZT-24
479.25	7.25	13.62	0.08	13.25	0.08	12.68	0.08	AZT-24
480.28	8.28	13.28	0.09	AZT-24
481.37	9.37	13.58	0.08	13.29	0.09	12.75	0.09	AZT-24
483.41	11.41	13.55	0.10	13.25	0.06	AZT-24
484.31	12.31	13.08	0.08	AZT-24
485.41	13.41	13.55	0.08	13.28	0.07	AZT-24
486.35	14.35	13.51	0.06	AZT-24
492.32	20.32	13.46	0.06	13.18	0.15	AZT-24
493.28	21.28	13.53	0.08	13.40	0.09	12.94	0.06	AZT-24
494.50	22.50	13.43	0.07	AZT-24
495.20	23.20	13.54	0.07	13.36	0.08	AZT-24
506.45	34.45	13.73	0.07	13.52	0.07	13.17	0.05	AZT-24
507.23	35.23	13.72	0.07	AZT-24
514.25	42.25	13.85	0.10	13.77	0.09	13.30	0.06	AZT-24
521.25	49.25	13.96	0.05	13.49	0.07	AZT-24
531.71	59.71	14.24	0.09	AZT-24
532.28	60.28	14.24	0.08	13.91	0.08	AZT-24
548.21	76.21	14.88	0.04	14.40	0.05	AZT-24
549.22	77.22	14.92	0.03	14.47	0.06	AZT-24
550.24	78.24	14.99	0.04	14.75	0.15	14.53	0.04	AZT-24
576.24	104.24	17.20	0.30	16.60	0.30	16.00	0.20	AZT-24
585.71	113.71	17.50	0.50	16.60	0.40	AZT-24
624.59	152.59	17.70	0.60	17.60	0.50	16.40	0.60	AZT-24
691.62	219.62	18.31	0.40	17.84	0.50	16.43	0.25	TNG/ARNICA
893.34	421.34	20.01	0.50	17.40	0.50	TNG/NICS

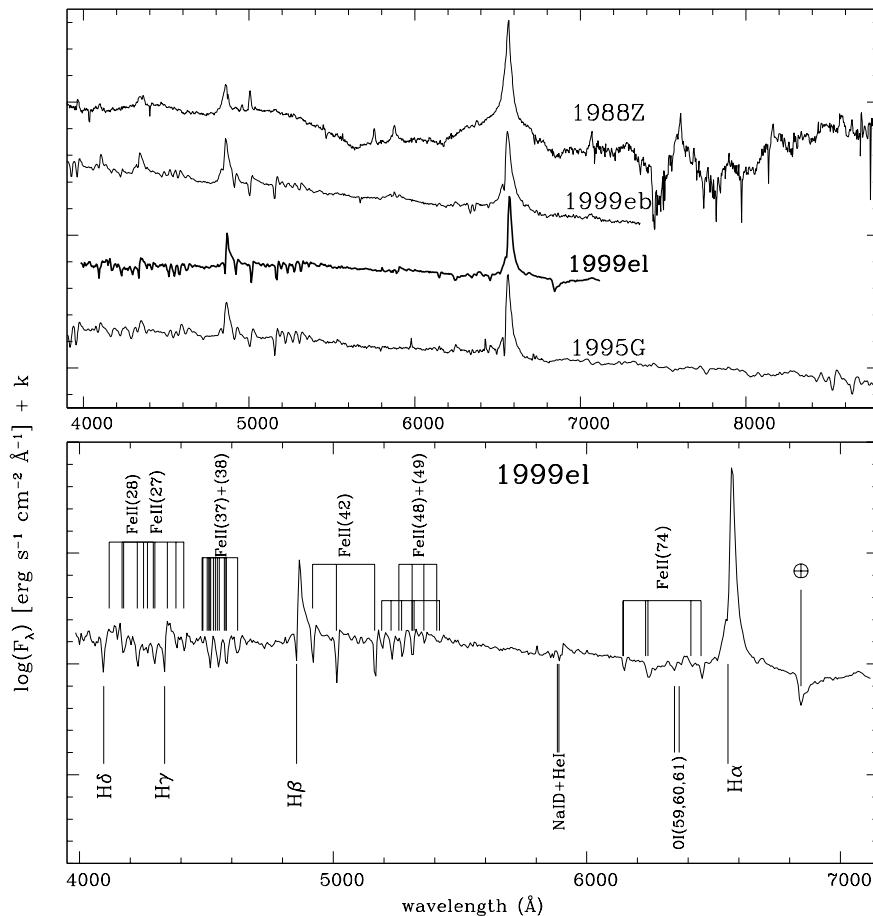


FIG. 2.—Identification of the lines on the optical spectrum of SN 1999el obtained on 1999 November 8 in Cananea (*lower panel*). Comparison with other SN spectra is shown in the upper panel. Vertical bars indicate the position of absorption lines blueshifted by $\sim 600\text{--}900\text{ km s}^{-1}$ with respect to the emission lines cores.

This absorption is commonly thought to arise from the CSM in the form of a wind.

3.2. Light Curves

Figure 3 shows the LCs at optical and NIR bands; we draw attention to some particular features. First, we see that a maximum of emission in the K band has not been observed. However, it seems that LC maxima in the other NIR and optical bands have been recorded. There are indications of small delays in the time of maxima occurrence that increase with a decrease of wavelength. During the first 90 days, the decline rate is quite fast, reminiscent of that of a Type II-L SN rather than that of a typical II_n SN, as already noted. After 90 days the LCs exhibit a much slower decrease, and, in particular, that of the K band flattens most. Since the K point at JD + 690 has been derived from a K_s measurement and any possible line contribution from CO emission is therefore excluded, the late behavior of the LC in K is not due to CO line emission. Note that this point has been derived from TNG observations, so the SN and its nearby sources are well resolved. The NIR LCs appear to remain flat up to JD + 893 (~ 420 days from the shock out-break), even if in the J band the decrease seems slightly faster than in the K band.

Figure 4 shows the time evolution of a series of color indices. We note the blueing in $J-H$ and $J-K$ during the first

~ 45 days (including ~ 10 days before the occurrence of maximum in the J band). Afterward, starting approximately around JD + 550, a reddening in $J-K$ and $J-H$ colors begins to be evident. The increase in errors that is significant after JD + 550 (affecting all colors) is due to the SN magnitude becoming comparable with that of the brightest of the nearby field stars, the two sources being difficult to deconvolve on the images from the smaller telescopes, even though we already noted that the K point obtained at late times from TNG images (JD + 690) is well established. This reddening effect is also evident as a flattening of the K light curve, whereas J and H are still slightly steeper in their decline (see Fig. 3) and can be attributed to an infrared excess arising at later phases. SN 1999el exhibits a more standard behavior in $B-R$, which increases after maximum and then flattens after ~ 70 days. This may be understood in terms of a cooling photosphere. In fact, the same trend seems to characterize all optical colors, with a change of ~ 0.5 mag in a period spanning ~ 200 days.

The behavior of the NIR emission can be followed on a color-color diagram ($H-K$ vs. $J-H$; see Fig. 5). Comparing the SN colors with the main-sequence locus (*solid line*), the blackbody locus (*dashed line*), and the reddening law (*arrow*), an NIR excess is evident even at early epochs, and this cannot be simply explained as reddened blackbody or stellar photospheric emission. After day 5, the colors evolve roughly along a track that appears almost parallel to the

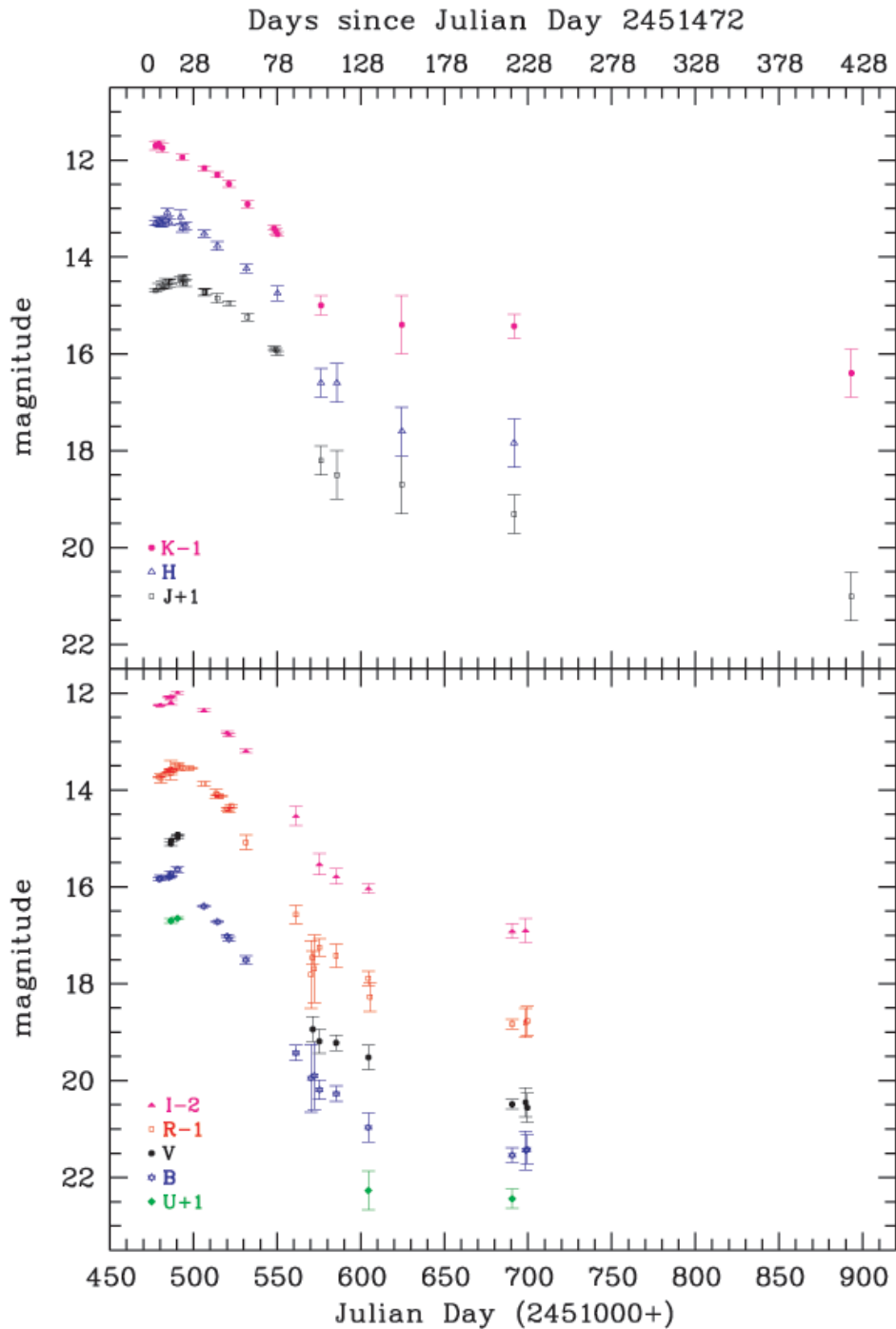


FIG. 3.—Optical and infrared LCs of the SN 1999el. Errors marked by the bars are those indicated in Tables 1 and 2.

reddening law, evolving as if A_V decreases with time. However, on day 219, a strong K excess is present. The most likely cause for the NIR excess is continuum emission from hot dust preexisting within the CSM of SN 1999el. Following Fassia et al. (2000), we can test this scenario in the following way. Given the (reddened) flux in the K band for day 5, 3.39×10^{-12} ergs cm^{-2} s^{-1} μm^{-1} , and the distance assumed in § 3.4, we can determine the radius of a blackbody surface emitting the same luminosity in K at 1500 K, roughly the dust sublimation temperature. It can be shown that reddening does not change the result by more than 10%–20%. This radius, 1.5×10^{16} cm, is comparable to the

light travel distance from the explosion time to day 5, $\sim 1.3 \times 10^{16}$ cm. Thus, the two independently determined distances are consistent with the presence of dust at a radius where it has not sublimated and radiates at IR wavelengths as a result of heating by UV photons from the original outburst.

3.3. Reddening

In order to give an estimate of the absolute luminosity of SN 1999el, it is necessary to determine its reddening. As can be seen in Figure 2, the interstellar lines of Na I cannot be re-

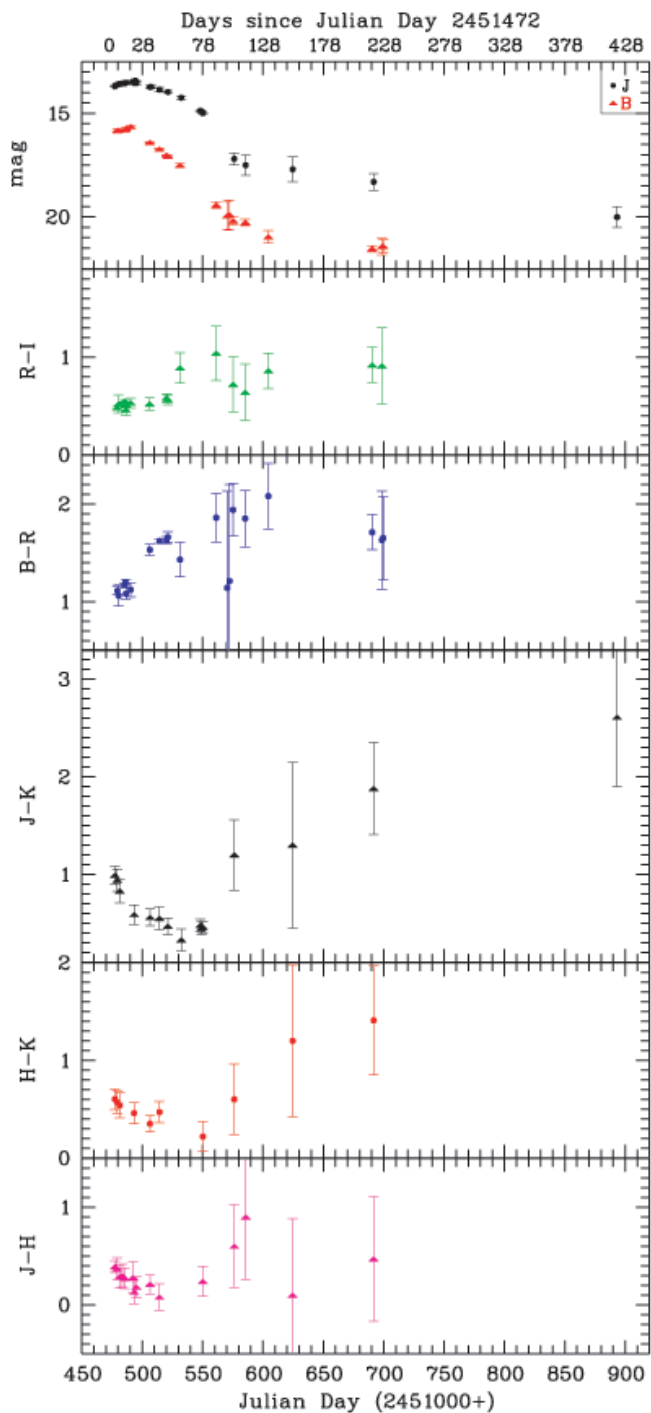


FIG. 4.—Optical and infrared colors of the SN 1999el. For the sake of comparison, in the upper box an optical (B) and an infrared (J) LC are displayed.

solved and therefore add little useful information. Hence, we can only assume the galactic value as a lower limit. From the maps of Schlegel, Finkbeiner, & Davis (1998) we obtain $A_B = 1.57$ mag. This map appears to systematically overestimate the extinction where $E(B-V) \geq 0.15$ mag, as pointed out by Arce & Goodman (1999). Since this occurs toward SN 1999el as well, we expect a lower galactic contribution to the extinction. We dereddened optical and NIR magnitudes using the interstellar extinction law given by Cardelli, Clayton, & Mathis (1989) and assuming an A_V ranging

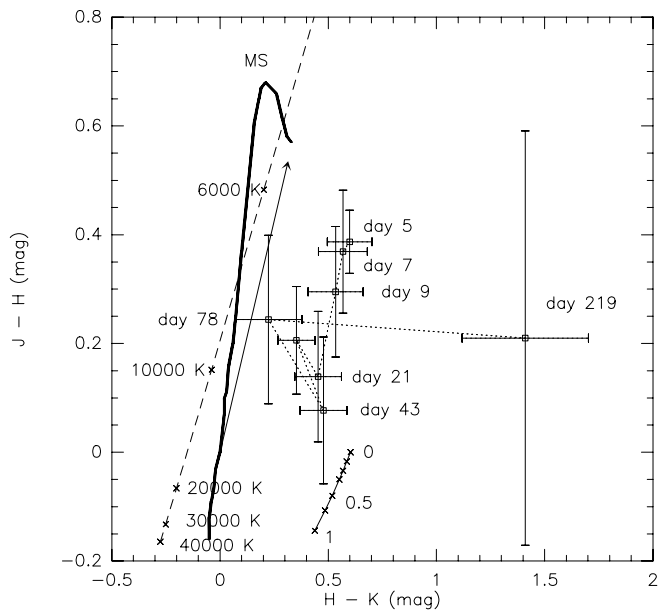


FIG. 5.—Color-color diagram ($H-K$ vs. $J-H$) showing the time evolution of the NIR emission of SN 1999el. The open squares (with error bars) mark the measured colors, which evolve along the dotted line from the 5th day from the discovery to the 219th day (the epoch is indicated near each data point). The solid black line reproduces the main-sequence locus from O6–8 to M8 stars (according to the colors given by Koornneef 1983), whereas the arrow from (0, 0) corresponds to a reddening $A_V = 5$ mag according to the standard law of Cardelli et al. (1989). The dashed line indicates blackbody colors with crosses at $T = 40,000, 30,000, 20,000, 10,000,$ and 6000 K. The effect of including Fe II line emission at 1.26 and $1.64 \mu\text{m}$ superposed on an NIR continuum (assumed from the JHK values on the 5th day) is shown by the solid line below the point of the 43rd day. The shifts are labeled in units (0, 0.5, 1) of the ratio of line-integrated emission at $1.26 \mu\text{m}$ to the overall K -band integrated continuum flux. For the sake of clarity, the line has been moved downward by 0.395 mag (i.e., the mark labeled as 0 actually falls over the point of day 5).

between 1.18 (corresponding to $A_B = 1.57$ mag) and 2.5 mag. These were then converted to fluxes according to Bessel (1979) and, in the NIR bands, the calibration given for the UKIRT standard. In Table 3 both apparent and absolute (dereddened) magnitudes at maxima are listed.

3.4. Blackbody Fits

We fitted a blackbody law to the dereddened fluxes in order to get estimates of the photospheric temperature. Since not all bands are covered on the same days, we con-

TABLE 3
APPARENT AND ABSOLUTE (DEREDDENED) MAGNITUDES FOR ALL OBSERVED PHOTOMETRIC BANDS

BAND	RELATIVE MAGNITUDE	ABSOLUTE MAGNITUDE	
		$A_V = 1.18$	$A_V = 2.50$
U	15.7	-18.3	-20.3
B	15.6	-18.1	-19.8
V	15.0	-18.3	-19.6
R	14.5	-18.5	-19.5
I	14.0	-18.7	-19.3
J	13.4	-19.0	-19.4
H	13.1	-19.2	-19.5
K	12.7	-19.5	-19.7

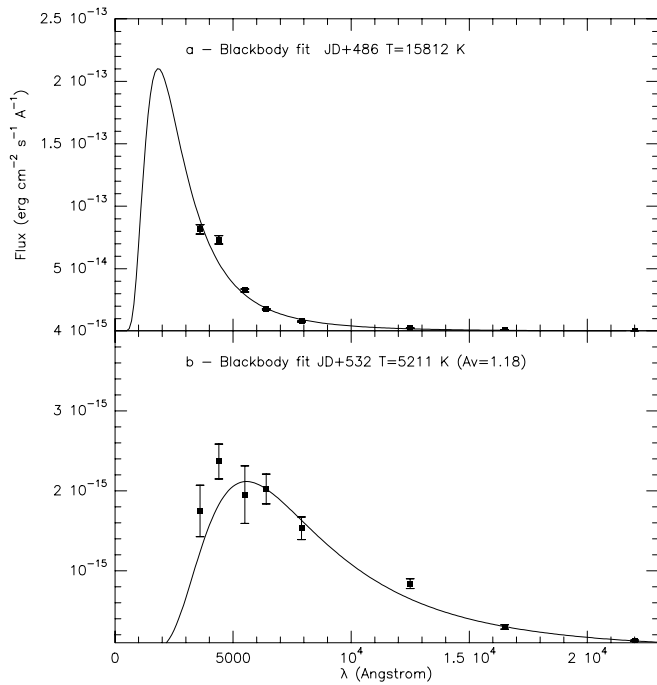


FIG. 6.—Blackbody fits to the dereddened fluxes for (a) JD + 486 (assuming $A_V = 2.50$ mag) and (b) JD + 532 (assuming $A_V = 1.18$ mag).

structured sets of *UBVRIJHK* fluxes complementing the available values with ones obtained through interpolation or using the results of spline fits to all data in a given wavelength. Then we adopted a one-parameter procedure for χ^2 minimization normalizing, for each selected day, all fluxes to that in the *R* band in order to remove the dependence on radius and distance. The *R* band was chosen because it is the better sampled band (see Table 1) and is likely to be much less affected by dust emission than the NIR bands. Two of the fits are shown in Figure 6 as examples of earlier and later epoch emission.

The resulting photospheric temperatures are listed in Table 4 and shown in Figure 7a for $A_V = 1.18$ and 2.5 mag.

TABLE 4
PHOTOSPHERIC TEMPERATURES FROM BLACKBODY CURVE FITS
FOR DIFFERENT EXTINCTIONS

JULIAN DAY	EPOCH (days)	TEMPERATURE (K)	
		$A_V = 1.18$	$A_V = 2.50$
479.....	7	7468 ± 2390	22370 ± 14717
485.....	13	7852 ± 2217	24254 ± 13135
486.....	14	7561 ± 1758	15812 ± 4901
490.....	18	7462 ± 1065	15066 ± 2629
495.....	23	6877 ± 534	12875 ± 1579
506.....	34	6533 ± 369	12245 ± 1488
514.....	42	5957 ± 310	9791 ± 871
521.....	49	5591 ± 389	9405 ± 1429
532.....	60	5211 ± 262	7683 ± 587
550.....	78	4699 ± 182	6488 ± 350
561.....	89	4997 ± 377	7262 ± 774
575.....	103	5419 ± 441	8220 ± 874
585.....	113	5145 ± 498	7586 ± 987
604.....	132	5029 ± 254	7457 ± 419
690.....	218	5660 ± 489	9487 ± 1480
698.....	226	4910 ± 205	7026 ± 474

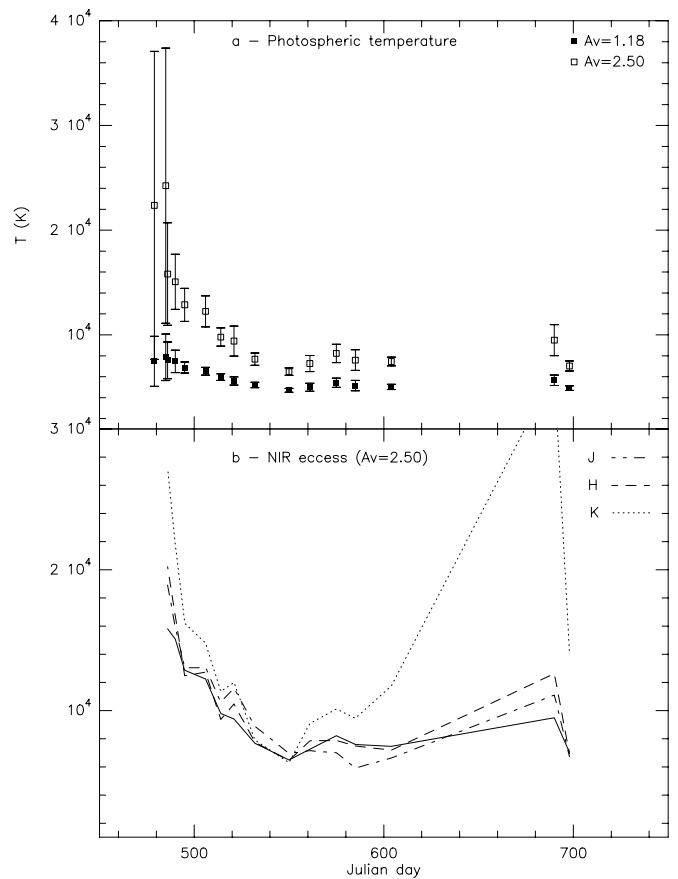


FIG. 7.—(a) Photospheric temperatures for different assumptions on the extinction. (b) Blackbody temperatures obtained from the NIR fluxes (for $A_V = 2.50$ mag) scaled using a dilution factor equal to the ratio of observed-to-blackbody flux in the *R* band, compared to the photospheric temperature (solid black line).

The temperatures for $A_V = 2.50$ mag are similar to those derived in the case of SN 1998S (Fassia et al. 2000); an extinction as large as $A_V = 3.00$ mag drives the photospheric temperature at early phases toward values that appear too high. Hence, A_V cannot much exceed ~ 2.5 mag, and $A_V = 1.18$ mag can be safely assumed as a lower limit.

We performed several tests in order to evaluate the quality of our fits. Most important, we repeated our procedure normalizing all fluxes to that in the *V* band. The differences between these newly obtained values and those listed in Table 4 increase with A_V , ranging from less than 6% for $A_V = 1.18$ mag to less than 20% for $A_V = 2.50$ mag. The most sensitive variations are observed on JD + 495 (temperatures from *V*-normalized data hotter by 23% for $A_V = 2.50$ mag than those from *R*-normalized data) and on JD + 506 (with a similar trend). Here two kinds of problems exist. First, when $\lambda T \gg hc/k$, a λ_0 -normalized blackbody flux tends to become equal to $(\lambda_0/\lambda)^4$ and no longer depends on temperature. This occurs for $T \gg 30,000$ K in the *V* band and $T \gg 40,000$ K in the *U* band. Then our fits are not reliable for very high temperatures. Second, differences in the results obtained by varying the normalization band may be related to the general increase in temperature found when excluding NIR fluxes from the fits (amounting, e.g., to up to 60% for $A_V = 2.50$ mag), although the trend shown in Figure 7a remains unchanged. This reflects physical differences in the regions that emit the bulk of radiation

at different wavelengths (particularly, in the optical and in the near-infrared). As an example, for SN 1998S, when fitting blackbody curves to optical spectra, Anupama, Sivarani, & Pandey (2001) find photospheric temperatures up to 30% hotter than those obtained by Fassia et al. (2000) from photometric data including NIR fluxes. We also repeated our fitting procedure excluding fluxes in the U band, where we have very few measurements. This yields somewhat higher temperatures but only at early epochs (20% on JD + 486 and 60% on JD + 490 for $A_V = 2.50$ mag); thereafter, differences amount to only a few percent. A major source of uncertainty is line emission in the photometric bands. Particularly at later stages (>100 days from LCs maxima), lines affecting the photometry in the I and R bands may develop (see Danziger et al. 1988) causing temperature underestimates.

The errors listed in Table 4 (calculated as the square root of the quadratic sum of the temperature residuals in the various bands) are largely dominated by those involving the NIR fluxes. We have already discussed the indication of an NIR excess from JHK colors. This is further demonstrated by plotting the blackbody temperatures obtained scaling the dereddened fluxes in the NIR to the ratio of observed-to-blackbody fluxes in the R band (which is equal to the square of the ratio of photospheric radius to distance). As shown in Figure 7b, higher NIR temperatures are derived at both early and late epochs. This may be reconciled if the NIR fluxes are not photospheric in origin but come from larger (cooler) regions starting soon after the explosion and continuing. Interestingly, an excess in the J band is exhibited until JD + 560 and is quite evident during the period (JD+)520–550 (see also Fig. 3); it corresponds to the noted bluing at early days. The K -band excess at late epochs is very strong, so much so that the flux has been left out when evaluating the error for JD + 604, JD + 690, and JD + 698. Fluctuations in the derived photospheric temperatures are appreciable in Figure 7a and may be related to the under-sampling of LCs in some bands (e.g., U and V). Unaccounted-for line emission may also contribute. The apparent warming during the period (JD+)550–600 coincides with the fading of the SN toward brightness values

similar to those of the brightest and closest star, and it may indicate that the two sources could not be accurately deconvolved at this epoch.

In conclusion, the photospheric temperatures derived from blackbody fits between (JD+)486–690 are mostly affected by uncertainties related to the unknown extinction, line emission within the photometric bands, and the degree of NIR excess. We believe that assuming $A_V = 1.18$ mag and $A_V = 2.50$ mag should result in lower and upper limits whose errors are otherwise not larger than those intrinsic to other similar studies (such as Fassia et al. 2000). Most significantly, the temporal evolution appears well defined.

3.5. Physical Parameters of the SN Photosphere

The photospheric radius was determined from the ratio of blackbody to observed fluxes in the R band. We slightly revised the distance to the host galaxy, assuming 26.3 ± 4.8 Mpc, from the distance modulus (32.1 ± 0.4 mag) we derived from our own observations of SN 2000E. Once the photospheric radius and temperature are known, the absolute bolometric luminosity can be estimated through the Stefan-Boltzmann law. A photospheric velocity was also derived as the ratio of radius to elapsed time from epoch 0. These data are listed in Table 5 in the cases $A_V = 1.18$ mag and $A_V = 2.5$ mag and shown in Figure 8. Quoted errors include the uncertainties in photospheric temperatures and measured fluxes, but not on the distance, since this would affect all data similarly. Note that increasing the photospheric temperature, e.g., by assuming larger extinctions, produces smaller radii and velocities; this confirms that A_V cannot much exceed the galactic value and rules out the occurrence of very high photospheric temperatures.

Qualitatively, the photospheric radius, velocity, and the bolometric luminosity exhibit the same behavior revealed by Fassia et al. (2000) for SN 1998S. The photospheric radius increases during the first 30 days, stays roughly constant until ~ 80 days from epoch 0, and then declines. The exact amount of the variations depends on the assumed extinction. The decrease in the photospheric velocity during the period 30–80 days is probably caused by the recession of

TABLE 5
PHOTOSPHERIC RADIUS, VELOCITY, AND ABSOLUTE LUMINOSITY FOR DIFFERENT EXTINCTIONS

JULIAN DAY	EPOCH (days)	$A_V = 1.18$			$A_V = 2.50$		
		Radius ($\times 10^{15}$ cm)	Velocity ($\times 10^3$ km s $^{-1}$)	Bolometric Luminosity ($\times 10^{43}$ ergs s $^{-1}$)	Radius ($\times 10^{15}$ cm)	Velocity ($\times 10^3$ km s $^{-1}$)	Bolometric Luminosity ($\times 10^{43}$ ergs s $^{-1}$)
479	7	1.6 ± 0.8	25.81 ± 13.09	$0.54^{+0.88}_{-0.51}$	0.74 ± 0.39	12.20 ± 6.37	$9.71^{+27.5}_{-9.68}$
485	13	1.5 ± 0.7	13.52 ± 5.80	$0.62^{+0.89}_{-0.57}$	0.73 ± 0.30	6.49 ± 2.70	$13.1^{+30.4}_{-12.9}$
486	14	1.6 ± 0.6	13.01 ± 4.75	$0.58^{+0.68}_{-0.50}$	1.0 ± 0.3	8.45 ± 2.46	$4.7^{+6.4}_{-4.1}$
490	18	1.7 ± 0.4	10.97 ± 2.49	$0.64^{+0.47}_{-0.44}$	1.1 ± 0.2	7.30 ± 1.23	$4.7^{+3.7}_{-3.2}$
495	23	1.9 ± 0.3	9.67 ± 1.35	$0.59^{+0.25}_{-0.27}$	1.3 ± 0.2	6.60 ± 0.91	$3.4^{+1.9}_{-1.9}$
506	34	1.8 ± 0.2	6.21 ± 0.65	$0.43^{+0.13}_{-0.15}$	1.2 ± 0.2	4.09 ± 0.55	$2.3^{+1.3}_{-1.3}$
514	42	1.9 ± 0.2	5.10 ± 0.52	$0.31^{+0.09}_{-0.11}$	1.3 ± 0.2	3.69 ± 0.42	$1.2^{+0.5}_{-0.5}$
521	49	1.8 ± 0.3	4.16 ± 0.60	$0.22^{+0.09}_{-0.10}$	1.2 ± 0.2	2.79 ± 0.56	$0.78^{+0.57}_{-0.52}$
532	60	1.7 ± 0.2	3.25 ± 0.39	$0.15^{+0.05}_{-0.05}$	1.3 ± 0.2	2.51 ± 0.32	$0.42^{+0.19}_{-0.19}$
550	78	1.4 ± 0.2	2.14 ± 0.22	$0.072^{+0.019}_{-0.023}$	1.2 ± 0.1	1.73 ± 0.18	$0.17^{+0.05}_{-0.06}$
561	89	0.9 ± 0.2	1.18 ± 0.23	$0.037^{+0.018}_{-0.009}$	0.70 ± 0.13	0.91 ± 0.18	$0.10^{+0.06}_{-0.06}$
575	103	0.5 ± 0.1	0.62 ± 0.12	$0.019^{+0.019}_{-0.010}$	0.42 ± 0.07	0.47 ± 0.08	$0.057^{+0.031}_{-0.032}$
585	113	0.6 ± 0.1	0.58 ± 0.14	$0.016^{+0.010}_{-0.010}$	0.44 ± 0.10	0.45 ± 0.10	$0.045^{+0.031}_{-0.030}$
604	132	0.48 ± 0.06	0.42 ± 0.06	$0.011^{+0.004}_{-0.004}$	0.36 ± 0.04	0.32 ± 0.04	$0.029^{+0.009}_{-0.011}$
690	218	0.24 ± 0.04	0.13 ± 0.02	$0.004^{+0.002}_{-0.002}$	0.17 ± 0.03	0.09 ± 0.02	$0.016^{+0.012}_{-0.011}$
698	226	0.33 ± 0.06	0.17 ± 0.03	$0.005^{+0.002}_{-0.002}$	0.26 ± 0.05	0.13 ± 0.02	$0.012^{+0.05}_{-0.06}$

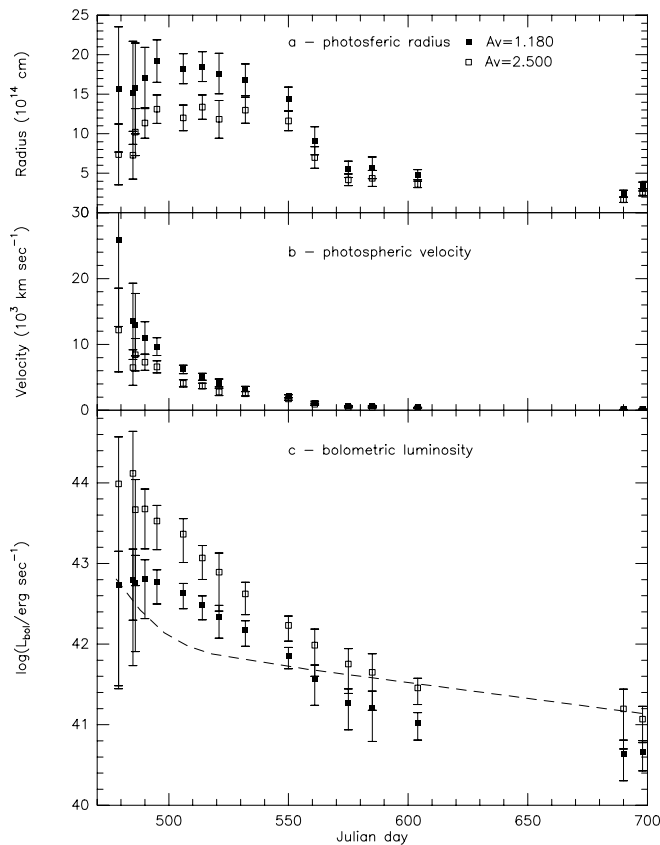


FIG. 8.—(a) Photospheric radius, (b) photospheric velocity, and (c) bolometric luminosity for different assumptions on the extinction. The dashed curve shows the radioactive decay luminosity of $0.07 M_{\odot}$ of ^{56}Ni .

the hydrogen recombination front through the expanding ejecta. However, an in-depth comparison is prevented by the uncertainty in the extinction of SN 1999el. Again, similarly to what was found for SN 1998S by Fassia et al. (2000), at around 100 days after outburst the light curve (see Fig. 8c) slows to the point of approximating the radioactive decay of ^{56}Co . As shown in Figure 8c, $0.07 M_{\odot}$ of ^{56}Ni (based on the relation given by Branch 1992 or direct comparison with SN 1987A) could power the luminosity at later epochs for $A_V = 2.5$ mag and can be assumed as an upper limit to the mass of ^{56}Ni produced by the explosion.

4. DISCUSSION

The early evolution (within ~ 100 days) of the light curves of SN 1999el indicates that this is one of the most rapidly declining SNe IIn among those studied so far. It is useful to compare its features with those of SN 1998S, the other recent and extensively observed SN IIn (Fassia et al. 2000). In the B band, SN 1999el exhibits a luminosity decrease even faster than that of SN 1998S and is more similar to a Type II linear SN than to previously studied SNe IIn, such as SN 1998Z or SN 1997ab. The light curves at various wavelengths of SN 1999el, with their steep decline, are closer to those of SN 1994aj (Benetti et al. 1999) and SN 1996L (Benetti et al. 1998) than to that of SN 1995G (A. Pastorello et al. 2002, in preparation), whose spectrum is, on the contrary, very similar to that of SN 1999el, as noted in § 3.1. Therefore, the indication of interaction with the CSM aris-

ing from the spectrum is not supported by the rapidly declining light curve. Consequently, SNe IIn seem to embrace a wide range of characteristics. Therefore, the differences between SN 1999el and SN 1998S are worth noting.

It appears that the SN 1998S LCs attain a maximum in the NIR some days after those in the optical bands (however, the precise times of occurrence for the optical maxima are uncertain since measurements appear to have begun when the optical light curve had already started declining). Conversely, in the case of SN 1999el the maximum emission in the NIR H and K bands occurs before that in the optical bands, whose maxima almost coincide with that in the NIR J band. The exact time of maxima at H and K bands is uncertain, but they seem to have occurred some time before the beginning of our observations. The differences may be appreciated by looking at the color curves shown in Figure 4. As previously noted, the evolution of $J-H$ and $J-K$ for SN 1999el exhibits an early appearance of an NIR excess (around day 5) and an NIR blueing effect in the first ~ 45 days. This seems observationally well established, since here the NIR LCs sample the SN when it was much brighter than the nearby sources c2 and c3 (see Fig. 1) and thus are easily measurable even though sometimes only partially resolved on SWIRCAM images. Although maxima at NIR wavelengths do appear to have been missed for SN 1998S, nevertheless there is no evidence for an early blueing effect in this case. Furthermore, an NIR excess from SN 1998S is not apparent at early epochs.

One possible origin of the quoted differences, in particular of the early NIR excess, may be due to an IR echo from pre-existing dust in the vicinity of SN 1999el not evaporated at the moment of the shock outburst. This would suggest that dust clumps near SN 1999el are distributed differently than those near SN 1998S, which may be devoid of nearby dust entirely. For SN 1998S this is supported by Leonard et al. (2000), whose spectroscopic observations suggest that the progenitor of SN 1998S underwent a major mass-loss episode that ended some 60 years before the explosion, followed by a mass-loss activity in the last 7 years before the explosion. If a mass-loss wind associated with the SN 1999el progenitor had never ceased before the time of explosion, the density of the CSM around it would be larger than in the case of SN 1998S.

In the above scenario, the interaction of the UV flash with the CSM around SN 1999el would have led to heating, destruction, and sublimation of dust. The extent of the region where grain sublimation and destruction can occur may be estimated as (see, e.g., Waxman & Draine 2000)

$$R_0 = 3.7 \times 10^{19} (Q_{\text{abs}} L_{49} a_{01}^{-1})^{1/2} \text{ cm}, \quad (1)$$

where Q_{abs} is the grain absorption efficiency at UV wavelengths, L_{49} the maximum luminosity in the range 1–7.5 eV in units of 10^{49} ergs s^{-1} (optical-UV flash) and a_{01} the mean size of grains in units of $0.1 \mu\text{m}$. Assuming $Q_{\text{abs}} \sim 1$ and $a_{01} \sim 1$, $R_0 \sim 10^{17}$ cm is obtained for a maximum luminosity of 10^{44} ergs s^{-1} (the greatest value indicated in Table 5), a distance which is 2 orders of magnitude larger than the largest photospheric radius attained by the supernova (see Table 5), but also somewhat greater than the estimate based on the occurrence of the NIR excess very early (see § 3.2). Since the grain destruction and sublimation due to the UV flash imply also the unlocking of Fe ions (if they exist in the

dust), we have been tempted to ascribe the early 45 days blueing to [Fe II] line emission. The [Fe II] lines that may affect *J* and *H* bands result from the transitions involving metastable levels $a^6 D_{9/2} - a^4 D_{7/2}$ ($\lambda = 1.26 \mu\text{m}$, $A = 5.6 \times 10^{-3} \text{ s}^{-1}$) and $a^4 F_{9/2} - a^6 D_{7/2}$ ($\lambda = 1.64 \mu\text{m}$, $A = 1.9 \times 10^{-3} \text{ s}^{-1}$), collisionally excited by free electrons (see Mouri, Kawara, & Taniguchi 2000 and references therein). Very large line-integrated fluxes (up to 0.5–1 times the continuum flux integrated on the *K* band; see Fig. 5) would be required to produce the observed changes in colors, indicating that [Fe II] lines alone cannot account for it. In addition, since relative luminosity of the main [Fe II] lines in the *J* and *H* windows is constant, the contribution of this mechanism to the color evolution is definitively ruled out.

If the early IR excess of SN 1999el is due to the presence of a CSM generated by a continuous wind of the progenitor star, it might be reasonable to expect its signature in the optical light curves. This seems not to be the case. Roscherr & Schaefer (2000) analyzed theoretically the modifications of optical LCs produced by echo processes. They assume spherical symmetry for the dust and find that critical parameters are r_{\min} , r_{\max} , and τ , where r_{\min} and r_{\max} are the inner and outer radii of the dust shell and τ the optical depth in the *R* band for a purely radial photon trajectory, a quantity directly related with the total mass of dust. Roscherr & Schaefer (2000) find that, in the case of thick shells, τ is the more sensitive parameter. Changes in τ effect changes in the luminosity of light maxima in various bands whose amounts depend on the wavelength range. Even the time at which the light maximum is attained may be shifted (by up to several days; B. Roscherr 2001, private communication) according to its wavelength. Unfortunately, these computations do not address the NIR bands. The decline rate is also strongly affected by changes in τ at levels once again dependent on wavelength. In this respect, a relevant parameter is the $\beta_{100,B}$ index, which corresponds to the luminosity drop in 100 days in the *B* band. Therefore, the $\beta_{100,B}$ index can provide information on the presence of a CSM around the SN. Observational data provide a value of $\beta_{100,B}$ greater than 4 mag for both SN 1999el and 1998S (about 4.8 and 4.3 mag, respectively). A comparison with the theoretical results quoted above suggests the surprising result that the expected amount of dust surrounding both SN 1999el and SN 1998S should be vanishingly small. (Or that almost all the preexisting dust is evaporated at the moment of the UV flash).

For SN 1999el this result is in contrast with the suggestion that the early IR excess is due to an IR echo caused by nearby dust.

We suggest that the failure of the $\beta_{100,B}$ index to display the presence of CSM around SN 1999el may be ascribed to the assumption made to derive theoretically this index, namely, the assumption of spherically distributed dust.

The theoretical results of Emmering & Chevalier (1988) on the IR echo light originated by an asymmetric CSM distribution around a SN progenitor clearly illustrate how many parameters influence the observed results. Indeed, they find that IR light curves can substantially change by varying the geometrical properties of a given nonspherical (but still axisymmetric) CSM distribution and/or its orientation relative to the line of sight. Even if not explicitly accounted for in their work, it can be nevertheless deduced that additional parameters, such as a nonradial density profile of the dust, play an additional pivotal role.

We intend in the future to provide a tentative model of the dust distribution around SN 1999el. Finally, we note that for both SN 1998S (Fassia et al. 2000) and SN 1999el, the observations do not rule out a scenario of dust formation after the explosion. In the case of SN 1999el, an occurrence like this would imply that the signature of dust appears at both early and also at late stages. In particular, for SN 1999el assuming $A_V = 1.18$ mag, the dereddened *K* magnitude on JD + 691 (see Table 2) yields an observed flux of $1.2 \times 10^{-13} \text{ ergs cm}^{-2} \text{ s}^{-1} \mu\text{m}^{-1}$. As in § 3.2, we can determine the radius of a blackbody-emitting surface for a temperature of 1500 K, which is roughly the sublimation temperature for dust grains. This amounts to $\sim 3 \times 10^{15} \text{ cm}$, on the order of the largest photospheric radius attained (see Table 5), a distance that might be covered by dust formed in the ejecta moving with a velocity $\sim 1600 \text{ km s}^{-1}$.

Therefore, the scenario we propose embraces the evolution of the progenitor star in that cold, high-luminosity, mass loss from evolved massive stars may proceed in episodes with asymmetric distributions. It is, however, conceivable that single mass-loss episodes are not completely stochastic in duration, periodicity, and intensity. Over long temporal intervals, possibly covering several cycles of activity, it is possible to define mean wind properties, such as, for example, the dependence of the mean mass-loss rate on the main structural parameters such as temperature and luminosity. If the SN explosion occurs during a long pause in mass loss, we observe a normal SN II; otherwise the typical features of the SNe IIn will appear with varying degrees of visibility.

5. CONCLUSIONS

Optical and NIR light curves have been presented for the Type IIn SN 1999el. These data, in comparison with those of SN 1998S, suggest that the progenitor star of SN 1999el was still undergoing a probably asymmetric mass loss episode at the moment of the explosion. Dust was already present in the expanding circumstellar envelope. Dust lying in the inner $\sim 10^{16} \text{ cm}$ evaporated at the outburst.

Later on, the evolution of NIR colors seems to be affected by the echo light from a preexisting asymmetrically expanding envelope. In the absence of mass loss, SN 1999el would have been presumably observed as a bona fide linear Type II SN. The way in which mass loss occurs in the last evolutionary phases of massive stars seems to be responsible for various observed departures of SNe II from the standard Type II-L and II-P behavior.

This paper is partially based on observations made with the Italian Telescopio Nazionale Galileo operated on the island of La Palma by the Centro Galileo Galilei of the CNAA (Consorzio Nazionale per l'Astronomia e l'Astrofisica) at the Spanish Observatorio del Roque de los Muchachos of the Instituto de Astrofísica de Canarias. The infrared data collected with the AZT-24 are products of the Supernova Watch-dogging Infrared Telescope (SWIRT), a joint project of the Astronomical Observatories of Collurania-Teramo (Italy), Pulkovo (Russia) and Rome (Italy). We thank F. Ghinassi and F. Mannucci for acquiring the latest NIR images with NICS. We warmly thank Bruce Roscherr for advice and suggestions about the echo light issue.

REFERENCES

- Anupama, G. C., Sivarani, T., & Pandey, G. 2001, *A&A*, 367, 506
Arce, H. G., & Goodman, A. A. 1999, *ApJ*, 512, L135
Aretxaga, I., Benetti, S., Terlevich, R. J., Fabian, A. C., Cappellaro, E., Turatto, M., & della Valle, M. 1999, *MNRAS*, 309, 343
Baffa, C., et al. 2001, *A&A*, 378, 722
Benetti, S., Cappellaro, E., Danziger, I. J., Turatto, M., Patat, F., & della Valle, M. 1998, *MNRAS*, 294, 448
Benetti, S., Turatto, M., Cappellaro, E., Danziger, I. J., & Mazzali, P. A. 1999, *MNRAS*, 305, 811
Bessel, M. S. 1979, *PASP*, 91, 589
Branch, D. 1992, *ApJ*, 392, 35
Cao, L., Qiu, Y. L., Qiao, Q. J., Hu, J. Y., Li, W., & Filippenko, A. 1999, *IAU Circ.*, 7288, 1
Cappellaro, E., & Turatto, M. 2001, in *The Influence of Binaries on Stellar Population Studies*, ed. D. Vanbeveren (Dordrecht: Kluwer), 199
Cappellaro, E., Turatto, M., Tsvetkov, D. Yu., Bartunov, O. S., Pollas, C., Evans, R., & Hamuy, M. 1997, *A&A*, 322, 431
Cardelli, J. A., Clayton, G. C., & Mathis, J. S. 1989, *ApJ*, 345, 245
Chugai, N. N. 1990, *Soviet Astron. Lett.*, 16, 457
———. 1992, *Soviet Astron. Lett.*, 36, 63
Chugai, N. N., & Danziger, I. J. 1994, *MNRAS*, 268, 173
D'Alessio, F., et al. 2000, *Proc. SPIE*, 4008, L703
Danziger, I. J., Bouchet, P., Fosbury, R. A. E., Gouiffes, C., Lucy, L. B., Moorwood, A. F. M., Oliva, E., & Rufener, F. 1988, in *Supernova 1987a in the Large Magellanic Cloud*, ed. M. Kafatos, & A. G. Michalitsianos (Cambridge: Cambridge Univ. Press), 37
Dopita, M. A., Cohen, M., Schwartz, R. D., & Evans, R. 1984, *ApJ*, 287, L69
Emmering, R. T., & Chevalier, R. A. 1988, *AJ*, 95, 152
Fassia, A., et al. 2000, *MNRAS*, 318, 1093
Hunt, L. K., et al. 1998, *AJ*, 115, 2594
Kohn, K., Kawabe, R., & Vila-Vilaró, B. 1999, *ApJ*, 511, 157
Koorneef, J. 1983, *A&A*, 128, 84
Landolt, A. U. 1992, *AJ*, 104, 340
Leonard, D. C., Filippenko, A. V., Barth, A. J., & Matheson, T. 2000, *ApJ*, 536, 239
Lisi, F., et al. 1996, *PASP*, 108, 364
Mouri, H., Kawara, K., & Taniguchi, Y. 2000, *ApJ*, 528, 186
Roscherr, B., & Schaefer, B. E. 2000, *ApJ*, 532, 415
Schlegel, E. M. 1990, *MNRAS*, 244, 269
Schlegel, D. J., Finkbeiner, D. P., & Davis, M. 1998, *ApJ*, 500, 525
Stathakis, R. A., & Sadler, E. M. 1991, *MNRAS*, 250, 786
Stetson, P. B. 1987, *PASP*, 99, 191
Terlevich, R. J. 1994, in *Circumstellar Media in the Late Stages of Stellar Evolution*, ed. R. E. S. Clegg, I. R. Stevens, & W. P. S. Meikle (Cambridge: Cambridge Univ. Press), 153
Turatto, M., Cappellaro, E., Danziger, I. J., Benetti, S., Gouiffes, C., & della Valle, M. 1993, *MNRAS*, 262, 128
Vinkó, J., et al. 2001, *A&A*, 372, 824
Waxman, E., & Draine, B. T. 2000, *ApJ*, 537, 796